Adhesion of Soft Membranes Controlled by Tension and Interfacial Polymers

Kheya Sengupta
CNRS, Aix-Marseille University, CINaM-UPR3118, Campus Luminy, Case 913 F-13288, Marseille, France

Laurent Limozin*
Adhesion and Inflammation Laboratory, CNRS UMR6212, Inserm UMR600, Aix-Marseille University, Campus Luminy, Case 937 F-13288, Marseille, France

(Received 7 October 2009; published 25 February 2010)

We examine experimental and theoretical aspects of nonspecific adhesion of giant vesicles on modified surfaces as model systems for cell spreading. Using dual-wave interference microscopy and new analysis, membrane undulations as well as large scale vesicle shape are monitored. Measurements and modelling show that the nucleation of adhesion depends critically on the interfacial polymer and membrane tension. Patch growth is governed by local membrane geometry, adhesion energy, and local viscosity. Finally, spreading stops when tension induced by adhesion unfolds excess membrane area.

DOI: 10.1103/PhysRevLett.104.088101 PACS numbers: 87.16.dj, 87.17.Rt, 87.64.M−

Adhesion of biological membranes, including that of cells, is of considerable fundamental and practical interest. It involves a combination of specific biochemical and generic physical interactions [1] and results from a balance between repulsive and attractive forces [2]. The role of fluctuations [3], membrane tension, and excess area [4] was recently evidenced, as was the crucial role of the polymeric pericellular coat in the early steps of adhesion. Giant unilamellar vesicles (GUVs) are often used to understand fundamental membrane processes and to test new micro-imaging techniques, ultimately dedicated to cellular studies. Static vesicle adhesion has been described in terms of an interaction potential [1,5], and the role of undulations has been recently emphasized [6]. Adhesion dynamics typically consists of three successive stages: nucleation, growth of the adhesion patch, and growth saturation [7–11]. Up to now, a universal experimental and theoretical description of these stages has been missing, even in the simplest case of generic forces.

In this Letter, we focus on adhesion dynamics of GUVs, driven by van der Waals attraction and tuned by a repulsive polymer cushion. We follow experimentally, using reflection interference contrast microscopy (RICM [12]), the three stages of adhesion and provide a theoretical basis for a quantitative description throughout. Dual-wave (DW)-RICM enables the determination of internal membrane tension σ via quantification of undulations in the prenucleation stage. A novel analysis enables correct reconstruction of membrane conformations for nonflat, semi-arbitrary shapes, allowing precise measurement of the adhesion energy and mechanical tension τ induced by an applied force. We discuss, in light of a recent theory [13], the difference between σ and τ, thus resolving a long-standing confusion in the measurement of membrane tension [5,14]. Next, calculating the interaction potential V and the energy to nucleate adhesion, we obtain an adhesion state diagram and show how nucleation depends critically on polymer density and initial tension. The growth stage is shown to be controlled by a balance of the driving force, arising from V, and geometry dependent dissipation in the polymer layer.

Experiment.—GUVs of radius 5–25 μm prepared using equimolar phosphatidylcholine (14:0) and cholesterol, and filled with sucrose at 200 mM, were sedimented in 250 mM salt buffer onto substrates coated with (i) avidin (denominated after ‘‘no-polymer’’), (ii) avidin and hyaluronic acid (HA) (‘‘sparse-polymer’’), (iii) polylysine and HA (‘‘dense-polymer’’) [15,16]. The GUVs are imaged with DW-RICM [12,16].

For each incident wavelength λ, the relation between local membrane-substrate distance h and the intensity I recorded in RICM, accounting for a finite illumination aperture [17] as well as reflections from multiple layers [15], is given by

$$I = S - D\frac{\sin z}{z}\cos\left\{\frac{4\pi n_1}{\lambda}\left[h\left(1-\sin^2\frac{\alpha_{\rm IA}}{2}\right)-h_0\right]\right\} \quad (1)$$

where S and D are the sum and difference of the theoretical maximal and minimal intensities, $\alpha_{\rm IA}$ is the illumination aperture angle, n_1 the refractive index of the medium, $z = \frac{4\pi n_1 h}{\lambda}\sin^2\frac{\alpha_{\rm IA}}{2}$, and h_0 is of the order of 40 nm [15]. Combining intensity measurement from two wavelengths, h is determined unambiguously in quasiflat zones by inverting Eq. (1) [16]. For the steeply ascending part of the membrane, the membrane profile is represented by a series of curved segments corresponding to each fringe, each defined by a radius of curvature and a tilt from the substrate. The profile is reconstructed fringe by fringe, starting from the substrate and writing the conditions of reflection on the curved interface and fringe formation using Eq. (1) [16].

Interaction potential.—The free energy of a vesicle next to a substrate is given by $F[h(\mathbf{r})] = \iint\{\frac{\kappa}{2}(\nabla^2 h)^2 + \sigma(\nabla h)^2 + V(h)\}d^2\mathbf{r}$ where κ is the bending rigidity

($\kappa \sim 100 k_B T$ [15]) and σ is the internal tension of the vesicle membrane [1]. The interaction potential $V(h)$ is a sum of lipid steric repulsion, vesicle weight, van der Waals attraction (Hamacker constant 2×10^{-21} J), repulsion due to membrane undulations [16]. Additionally, there is the steric repulsion by the polymer layer which depends on the surface density and the polymer Flory radius (~100 nm) [16].

The shape of $V(h)$ results essentially from the balance of van der Waals attraction and polymer repulsion. With increasing polymer density, it exhibits first one deep minimum [state 1, strong adhesion, Fig. 1(a)]; then a secondary shallow minimum appears at $h > 100$ nm (state 2, weak and strong adhesion); at high polymer density, only the shallow minimum at $h > 100$ nm remains (state 3) [Fig. 1(a)]. Experimentally, state 3 is realized in the dense-polymer, state 1 in the no-polymer, and state 2 in the sparse-polymer case. The energy of the deep minimum of V was compared with the adhesion energy W measured on adhering vesicles, using Young-Dupré relation $W = \tau(1 - \cos\theta)$, with the contact angle θ and mechanical tension τ, which is obtained by local balance with bending in the adhesion rim [18]. We obtained for no-polymer $W \sim 1.5 \times 10^{-5}$ J/m^2 and for sparse-polymer $W \sim 2 \times 10^{-6}$ J/m^2 in agreement with the predicted values of V [Fig. 1(a)].

Prenucleation state.—Following sedimentation, vesicles reside transiently in the shallow minimum of V, in a state of weak adhesion. They hover on a cushion of trapped liquid of thickness $h_c \sim 100$–200 nm and form a flat contact zone of radius R_c. The membrane exhibits strong undulations (out-of-plane fluctuations) whose amplitude is related to the internal membrane tension σ and the stiffness of the potential $\frac{\partial^2 V}{\partial h^2}$ [1]. Typically, the measured amplitude is about 15 nm which corresponds to an internal tension $\sigma \sim 10^{-5}$ N/m [16].

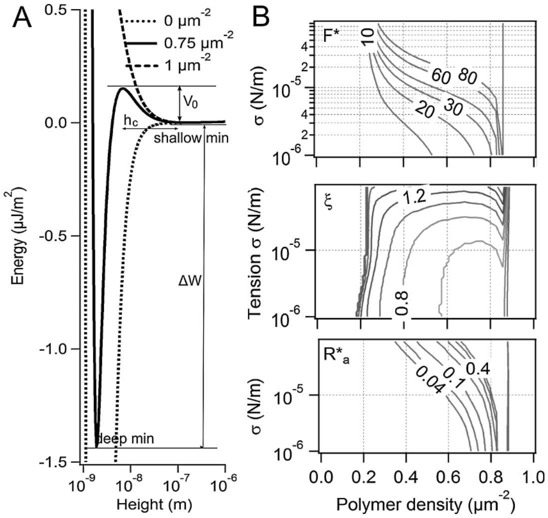

FIG. 1. (a) Calculated interaction potential depends on polymer density. (b) Energy barrier for nucleation of adhesion, F^* ($k_B T$), transition size between adhered and nonadhered zone, ξ (μm), and nucleation radius, R_a^* (μm) depend on polymer density and internal membrane tension.

An alternative measurement of tension arises from application of an external force—this is the mechanical tension τ. In the prenucleated state, τ can be measured by balancing it against gravity g which gives, in the capillary approximation, $\tau \sim (4/3)\Delta\rho g R_v^4 / R_c^2$ [14,19], with $\Delta\rho$ the vesicle specific density and R_v the vesicle radius at the equator. Depending on vesicle size and initial excess area, τ is in the range $10^{-7} - 10^{-6}$ N/m, much lower than σ. The difference between σ and τ is consistent with a recent theoretical description [13] which predicts that $\sigma \simeq \tau + \sigma_0$, where $\sigma_0 = kT/8\pi a^2 = 6 \times 10^{-6}$ N/m, $a \sim 0.2$ nm^{-1} being a wave vector upper cutoff. Finally, with this understanding of tension and using Young-Dupré relation, the effective adhesion energy induced by gravity is about $10^{-8} - 10^{-7}$ J/m^2.

Nucleation.—In case V exhibits a deep minimum (no-polymer or sparse-polymer), the membrane, initially in the shallow minimum, eventually nucleates an adhesion patch in the deep minimum. The nucleation depends on the barrier height V_0, its distance to the shallow minimum ($\sim h_c$), and the adhesion energy difference ΔW between the two minima [Fig. 1(a)] [20]. Let ξ be the lateral transition size on which the membrane passes from the shallow to the deep minimum. Minimization of the total free energy F, with respect to the radius of an adhesion patch, gives the critical adhesion radius as $R_a^* = F_0/(2\xi\Delta W)$, with $F_0 = V_0(\xi_\kappa^4/\xi^2 + \xi_\sigma^2 + \xi^2)$, $\xi_\kappa = (\kappa h_c^2/V_0)^{1/4}$, $\xi_\sigma = h_c\sqrt{\sigma/V_0}$. The corresponding energy of nucleation is $F^* = F_0(1 + R_a^*/2\xi)$ which should be maximized in order to determine ξ numerically. In the limit $V_0 \ll \Delta W$, and in the rigidity dominated regime, the classical results $\xi \simeq \xi_\kappa$ and $F_0 \sim \sqrt{\kappa V_0 h_c^2}$ [1,2,20] are retrieved. In the general case, F^* is represented in Fig. 1(b). The time of nucleation scales as $\exp(F^*/k_B T)$, and, in contrast to previous prediction [10], increases strongly with increasing tension. Thus, the nucleation time between two vesicles differing in tension by a factor 2 increases by about $\sim \exp(3) \sim 15$.

The predicted values of ξ and R_a^* [Fig. 1(b)] are in agreement with measurements from RICM images, which give $\xi = 0.7$–1.6 μm, and $R_a^* = 0.7$–1.8 μm (the latter is slightly higher than expected, possibly due to limited spatial and temporal resolution).

Growth of adhesion patch.—We examine now the situation where a patch nucleated at time $t = 0$ grows larger than the critical radius R_a^*. In analogy to droplet spreading, the growth law is set by balancing gain in adhesion energy with viscous dissipation in the outer medium near the contact line [8,21]

$$U = \frac{dR_a(t)}{dt} = \frac{\tan\theta(t)}{c\nu}\Delta W \tag{2}$$

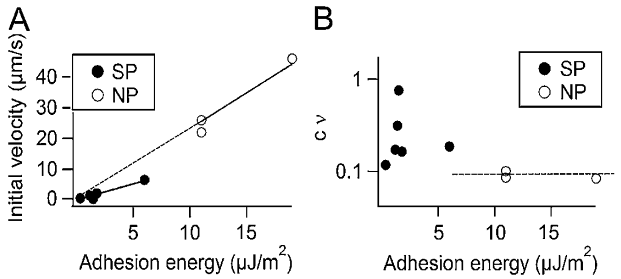

FIG. 2. (a) Initial spreading velocity in each case (SP: sparse-polymer and NP: no-polymer) is proportional to adhesion energy W_f, as predicted by Eq. (2). (b) Viscosity is higher on SP. The dashed line indicates the viscosity of water.

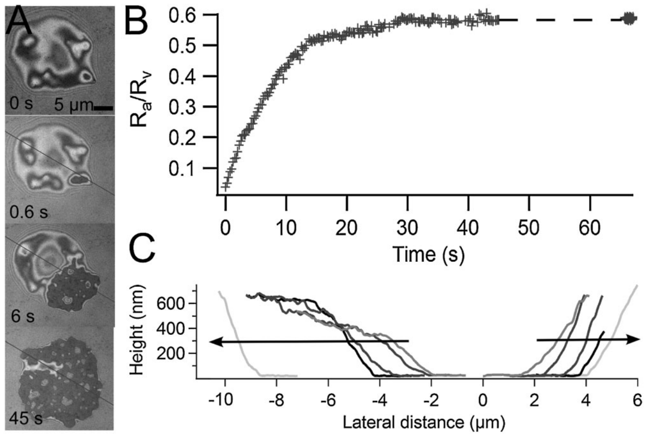

FIG. 3. Initially floppy vesicle F adhering on a sparse-polymer layer. (a) Successive RICM snapshots. (b) Time evolution of the adhesion radius. (c) Successive membrane profiles (time: 0.6, 3.7, 6.2, 8.7, 45 s).

where U is the growth velocity, $R_a(t)$ the instantaneous radius of the adhesion patch, $\Delta W = W_f - W_i$ is the difference between adhesion energies in the deep (final state) and shallow minimum (initial state), c is a numerical constant of order 10–100, ν is the local viscosity of the external medium, and $\theta(t)$ is the local contact angle. Two limiting cases have been previously described theoretically [10,11,21], corresponding to the classical situations of (a) *spreading* of a liquid droplet where the contact angle increases with time, or (b) *dewetting* of a liquid film, where the contact angle remains constant. In practice, however, the initial nucleation patch always subtends a local contact angle of order $h_c/\xi \simeq 0.2$ [7]. Furthermore, from measured values, $W_f \gg W_i$. Therefore, since for a given system $c \times \nu$ is roughly constant, a linear dependence of the initial velocity on W_f is expected and is indeed observed [Fig. 2(a)]. Plotting $\frac{W_f \tan\theta}{U}$ at the onset of growth as a function of W_f [Fig. 2(b)] gives an estimate of $c\nu$. Setting $c \simeq 100$, the friction in the no-polymer case corresponds to the viscosity of water [dashed line, Fig. 2(b)], while, in the sparse-polymer case, the relative viscosity is increased [Fig. 2(b)].

We now focus on two typical examples of GUVs of similar size adhering on sparse polymer. For a floppy vesicle (Fig. 3, vesicle F of radius $R_v = 22$ μm, $W_f = 1.8 \times 10^{-6}$ J/m^2), the initial tension is low ($\tau \sim 2 \times 10^{-7}$ N/m) resulting in a large cushion $R_c = 12$ μm [Fig. 3(a)]. Nucleation occurs, within seconds after sedimentation, at the edge of the contact zone, resulting in an asymmetric spreading geometry. The shape of the membrane [Fig. 3(c)] towards the interior of the contact zone clearly shows the presence of a liquid cushion which is in the process of being expulsed or dewetted (with measured angle $\theta \sim 0.2$ rad). For a vesicle initially more tense (Fig. 4, vesicle T, $R_v = 17$ μm, $W_f = 1.4 \times 10^{-6}$ J/m^2), $\tau \sim 5 \times 10^{-7}$ N/m and $R_c = 3$ μm. As expected for a tense vesicle, nucleation is delayed (by few minutes). The growth behavior is initially dewetting-like (θ constant at $\sim$0.2 rad). After about 1 s, the growth switches to spreading-like—the angle starts increasing, as indicated by a change of slope in the adhesion growth curve [arrow in Fig. 4(b)], as well as by the shape of the membrane profile [Fig. 4(c)]. The tension, measured throughout the growth regime, is seen to be roughly constant and increases only into the saturation regime.

Whether the growth of the adhesion patch proceeds by dewetting or droplet-like spreading depends on geometry through the value of the spreading index $\chi = (R_a(t) + \xi)/R_c$. Initially, $\chi = \chi_i = (R_a^* + \xi)/R_c$ depends only on the radius of the vesicle and its mechanical tension τ in the prenucleation state [Fig. 5(a)]. For small vesicles or large τ, $\chi_i > 1$, and the initial growth is like droplet spreading. For large floppy vesicles, as is always the case here, $\chi_i < 1$, and initial growth is dewetting-like, governed by Eq. (2) with $\theta = 0.2$. When $R_a(t)$ overtakes R_c, χ exceeds 1, signalling a switch to droplet-like spreading—θ increases in Eq. (2) and accelerates the growth. For vesicle T, the

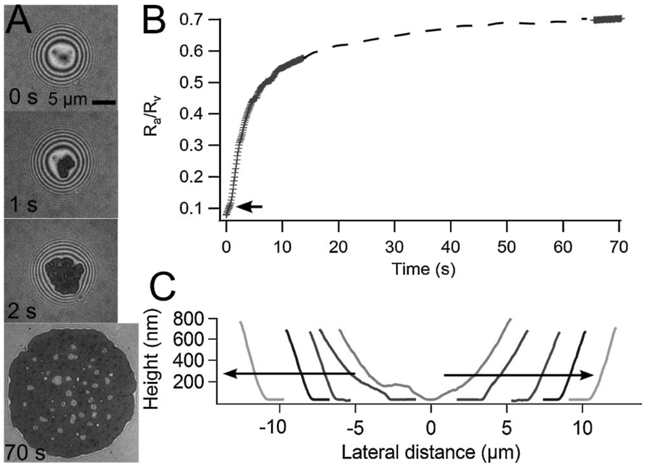

FIG. 4. Initially tense vesicle T adhering on a sparse-polymer layer. (a) Successive RICM snapshots. (b) Time evolution of the adhesion radius. (c) Successive membrane profiles (time: 0, 1, 3, 4, 14 s).

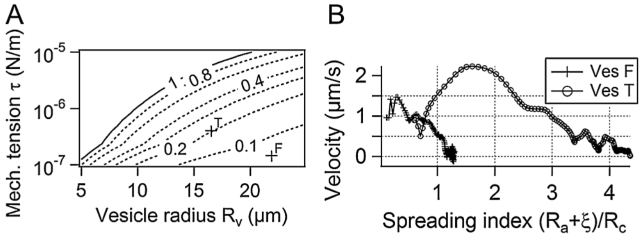

FIG. 5. (a) Isolines of the initial spreading index χ_i for a polymer density of $0.75/\mu\mathrm{m}^2$. Points *F* and *T* show parameters for the two vesicles detailed in Fig. 3 (F) and Fig. 4 (T). (b) Spreading velocity as a function of spreading index for vesicles F and T.

velocity increases for $\chi > 1$ when the vesicle enters droplet spreading-like growth, showing that dewetting and droplet-like spreading are not fundamentally different [Fig. 5(b)].

Saturation of growth.—Saturation is set by the microscopic membrane excess area α, which is related to the internal tension σ. The difference in the macroscopic excess area δA between the initial (i) and final (f) state of spreading is given by [21]

$$\delta A_f - \delta A_i = \alpha_i - \alpha_f = \frac{kT}{8\pi\kappa} \ln\left(\frac{\sigma_0 + \tau_f}{\sigma_0 + \tau_i}\right) \tag{3}$$

where we have rewritten σ in terms of τ and σ_0. If the global vesicle shape is a spherical cap, $\delta A \sim \theta^4/16$ with θ the contact angle [19]. Estimating $\theta_i = \arcsin(R_c/R_v)$, τ_i from the balance with gravity [19], θ_f from direct measurement, and τ_f from local balance of tension and bending (range $7 \times 10^{-6} - 7 \times 10^{-5}$ N/m), Eq. (3) is seen to hold for all vesicles studied within a factor 5 (for $\sigma_0 = 10^{-6}$ N/m) or 10 (for $\sigma_0 = 6 \times 10^{-6}$ N/m). The lack of a better match may arise from the failure of the spherical cap approximation [16]. Simultaneously solving Young-Dupré law and Eq. (3) for τ_f and θ_f allows prediction of the final state.

Conclusion.—We have outlined the first complete quantitative description of vesicle adhesion driven by generic forces, emphasizing the role of membrane tension and glycocalyx-like polymers. Though the three stages of nucleation, growth, and saturation are, in principle, well separated, we show that due to overlap of the growth regimes, power laws without limit between regimes [10] are insufficient to describe even the simple case of generic interactions. Our integrated approach yields new features in each stage of adhesion: (i) tension increases nucleation time by limiting membrane deformation thus restricting membrane-substrate contacts, (ii) growth behavior is dictated by local viscosity and local contact angle through the spreading index, (iii) saturation of growth occurs after unfolding of the membrane excess area by the applied mechanical tension. In a reverse manner, microscopic quantities, including interaction potential and polymer-coat viscosity, can be deduced from our measurements [22]. Several possible complications have not been dealt with: formation of a dimple in the contact zone following sedimentation, beginning of nucleation before the end of sedimentation, a nonsmooth adhesion rim, and multi-nucleations. The quantitative approach presented here is expected to serve as a basis for studying the more complicated case of specific ligand-receptor mediated adhesion and, ultimately, adhesion of cells.

We thank P. H. Puech, C. Z. Zhang, Z. G. Wang, J. B. Fournier, M. P. Valignat for fruitful exchanges and P. H. Puech for critical reading of the manuscript.

---

*laurent.limozin@inserm.fr

[1] R. Lipowsky, *Handbook of Biological Physics* (Elsevier, Amsterdam, 1995), pp. 521–602.
[2] E. Sackmann and R. F. Bruinsma, Chem. Phys. Chem. **3**, 262 (2002).
[3] A. Zidovska and E. Sackmann, Phys. Rev. Lett. **96**, 048103 (2006); A. Pierres *et al.*, Biophys. J. **94**, 4114 (2008).
[4] D. Raucher and M. P. Sheetz, J. Cell Biol. **148**, 127 (2000).
[5] J. Radler *et al.*, Phys. Rev. E **51**, 4526 (1995).
[6] E. Reister-Gottfried *et al.*, Phys. Rev. Lett. **101**, 208103 (2008).
[7] R. Bruinsma *et al.*, Phys. Rev. E **61**, 4253 (2000).
[8] A. Bernard *et al.*, Langmuir **16**, 6809 (2000).
[9] A. Boulbitch *et al.*, Biophys. J. **81**, 2743 (2001); D. Cuvelier and P. Nassoy, Phys. Rev. Lett. **93**, 228101 (2004).
[10] P. Puech *et al.*, Biophys. Rev. Lett. **1**, 85 (2006).
[11] P. De Gennes *et al.*, Langmuir **19**, 7112 (2003).
[12] L. Limozin and K. Sengupta, Chem. Phys. Chem. **10**, 2752 (2009).
[13] J.-B. Fournier and C. Barbetta, Phys. Rev. Lett. **100**, 078103 (2008).
[14] U. Seifert, Phys. Rev. Lett. **74**, 5060 (1995).
[15] L. Limozin and K. Sengupta, Biophys. J. **93**, 3300 (2007).
[16] See supplementary material at http://link.aps.org/supplemental/10.1103/PhysRevLett.104.088101 for details of the methods and numerical values of parameters.
[17] J. Radler and E. Sackmann, J. Phys. II (France) **3**, 727 (1993).
[18] A. Albersdorfer *et al.*, Biophys. J. **73**, 245 (1997).
[19] P.-H. Puech and F. Brochard-Wyart, Eur. Phys. J. E **15**, 127 (2004).
[20] C.-Z. Zhang and Z.-G. Wang, Phys. Rev. E **77**, 021906 (2008); personal communication.
[21] F. Brochard-Wyart and P. De Gennes, Proc. Natl. Acad. Sci. U.S.A. **99**, 7854 (2002).
[22] P. Robert *et al.*, Biophys. J. **95**, 3999 (2008).